https://doi.org/10.48048/tis.2024.7760

Identification of Soil Fracture Zone Using Waxman-Smits Model Based on ERT Survey Data

Budy Santoso[1,2,*], Hendarmawan[3] and Yudi Rosandi[2]

[1]*Department of Geophysics, Universitas Padjadjaran, Sumedang 45363, Indonesia*
[2]*Study Program of Doctor of Environmental Sciences, Universitas Padjadjaran, Sumedang 45363, Indonesia*
[3]*Department of Geological Engineering, Universitas Padjadjaran, Sumedang 45363, Indonesia*

([*]Corresponding author's e-mail: budi@geophys.unpad.ac.id)

Received: 23 November 2023, Revised: 22 December 2023, Accepted: 29 December 2023, Published: 30 May 2024

Abstract

Fracture is an early symptom of ground movement related to the physical properties of soil, including permeability, porosity, density, cohesion and internal friction angle, where these physical properties affect the stability of the soil. This research aims to identify soil fracture in landslide-prone areas using the values of water saturation and soil pressure based on electrical resistivity tomography (ERT) data. Water saturation values are obtained using the Waxman-Smits model based on the relationship between porosity and resistivity. The advantage of this model is its ability to apply correction due to clay-containing soil layers found in the research area. Another parameter used to determine soil fracture is the soil stress value. In this study, the Rankine method is used to calculate soil stress, and this method can be applied to the soil conditions that experienced deformation, caused by weathering of breccia and tuff rocks, allowing water to penetrate the rock medium. Consequently, the weathered layers of breccia and tuff act as slip planes. The presence of water on the slip planes leads to soil movement. Based on the analysis results, soil fractures are correlated with low water saturation values and contrast in soil stress values. A profound contrast in water saturation and soil stress values appears only at fractured slopes. Based on our analysis, soil fractures correlate with low water saturation values (5 - 15 %) accompanied by apparent contrast of soil stress values, i.e. the fractured soil is having lower soil stress (< 15 KN/m^2) in comparison to the surrounding. Such a contrast was not found in slopes without fractures.

Keywords: Fracture, ERT, Rankine method, Soil stress, Waxman-Smits model, Water saturation

Introduction

The initial signs of ground movement can be observed through the presence of fractures in unstable soil. Unstable soil refers to soil that is prone to soil movement, deformation or slope failure. Factors contributing to soil instability may include geological conditions, water content, slope steepness and human activities. The existence of fractures indicates the presence of significant tensile stress within a specific zone [1]. Fractures at the research site can be identified based on the values of soil resistivity, water saturation and soil stress. According to the initial hypothesis, fractures have higher resistivity values compared to the surrounding soil or rocks, except for the bedrock. Soil resistivity has a strong correlation with soil fractures [2] because during the process of fracturing, the initially saturated soil with low resistivity experiences a decrease in water content as it dries out, resulting in the formation of fractures accompanied by a significant increase in resistivity values. Soil resistivity is related to water saturation and soil stress, hence all of these 3 data are required to identify fractures. Water saturation values can be obtained from resistivity data using the Waxman-Smits equation, while soil stress can be indirectly derived from the inverted resistivity data. One geophysical method that can determine resistivity contrasts in the soil is electrical resistivity tomography (ERT).

ERT research for fracture identification has been widely conducted, but it has mostly been limited to physical simulations of soil samples. Some examples include ERT measurement experiments for reconstructing complex fracture patterns and computational modeling using clay soil samples [3], the application of ERT for identifying soil fractures in sand layers through physical simulations in the laboratory [4], and the implementation of ERT methods to detect fractures in engineered cement composites under monotonically uniaxial stress [5]. The *in-situ* application of ERT for fracture identification in potentially landslide-prone areas has been relatively unexplored. Some previous ERT studies conducted include measurements for landslide identification on unstable slopes using a soil fracture approach [6], and

ERT measurements at a cracked flood embankment site in the Hull area of England utilizing both 2D and 3D electrode configurations [7].

Fractures usually occur on disturbed or landslide-prone slopes. The ERT method can be applied to monitor disturbed slopes, where the slope may experience collapse triggered by rainfall. The ERT method can also be used to monitor variations in subsurface water content [8], to assess slope conditions such as identifying slope deformations [9], determining sliding planes [10-12] and determining the subsurface lithology of slopes [13].

Soil fractures are related to the water content (saturated/unsaturated) within the soil. Water saturation can be determined based on petrophysical models, such as the Archie and Waxman-Smits models, which describe the relationship between porosity and resistivity [14-17]. The Archie and Waxman-Smits petrophysical models have been widely used to calculate water saturation based on well logging data in hydrocarbon exploration [18,19]. However, the application of these petrophysical models for determining indications of fractures is still limited. The Archie petrophysical model, although capable of explaining the relationship between porosity and resistivity, i.e. the application is limited only to the sandy formations without clay or shale content [11]. In the Archie equation, clay is considered an impurity that can affect resistivity values as it is conductive in nature.

Water-filled fractures exert high stress, pushing the mass out of the slope and causing soil movement. The presence of water in the fractures softens the soil, reducing its strength. The position and depth of the fractures, as well as the saturated soil layers, can be identified from the active soil stress profile and the water saturation profile. Therefore, by using the relationship between resistivity data, water saturation and soil stress, estimates can be obtained for the layers of soil experiencing fractures, soil settlement and water saturation. Dry soil layers and saturated soil significantly affect the magnitude of vertical and lateral soil stress. The magnitude of lateral soil stress depends on several factors, including the physical properties of the soil, soil shear strength, interaction between soil and geological structures and external loads that affect soil strength.

Until now, research on fracture identification has primarily focused on using resistivity data, while the use of soil stress and water saturation data for studying fractures has not been extensively explored. Therefore, we conducted this research to understand the relationship between resistivity data, water saturation and soil stress in identifying soil fractures.

Materials and methods

Rainfall intensity data

Based on the rainfall data in the research area (Sumedang Regency and surrounding areas), there has been moderate and light rainfall over a relatively moderate duration. In several highland areas with moderate to high slope gradients, this could trigger soil instability and result in landslides. The rainfall data obtained from the Meteorology, Climatology and Geophysics Agency from December 15, 2022, to December 22, 2022, is presented in **Table 1**.

Table 1 Rainfall data in the Cimanggung area, Sumedang Regency [20].

Date	Rainfall (mm)	Explanation
12-15-2022	0	Cloudy
12-16-2022	34	Moderate rain
12-17-2022	18	Light rain
12-18-2022	32.5	Moderate rain
12-19-2022	8	Light rain
12-20-2022	11.5	Light rain
12-21-2022	7.6	Light rain
12-22-2022	7.5	Light rain

Geomorphology and geological setting

The research site is located in undulating hills at an elevation ranging from 684 to 770 m above sea level, with slope angles ranging from 30 - 40 °, forming a V-shaped morphology known as a horseshoe shape. Based on the classification of slope angle classes, the research site falls within the category of very steep hill morphology [21]. The land use in the northern and southern areas consists of relatively dense

residential settlements. Therefore, if there are soil fractures present at this location, it can significantly impact the stability of the soil, posing a threat to the safety of the residents living in these settlements.

The vulnerability level of ground movements in the research area is within the medium-high ground movements vulnerability zone, this means that the location has the potential for landslides, especially during periods of high rainfall, particularly in areas bordering rivers, valleys and disturbed slopes. The map depicting the Vulnerability to landslide zone map of the study area is shown in **Figure 1**. Landslides occur in areas with sparse vegetation, moderately to steep slopes, and are associated with young volcanic rock formations and moderate to high rainfall. The research area falls within the category of areas with sparse vegetation and moderately to steep slopes, indicating the potential occurrence of both new landslides and reactivation of old landslides. The presence of soil or rock fractures can serve as an indicator of the potential occurrence of new landslides or reactivation of old landslides.

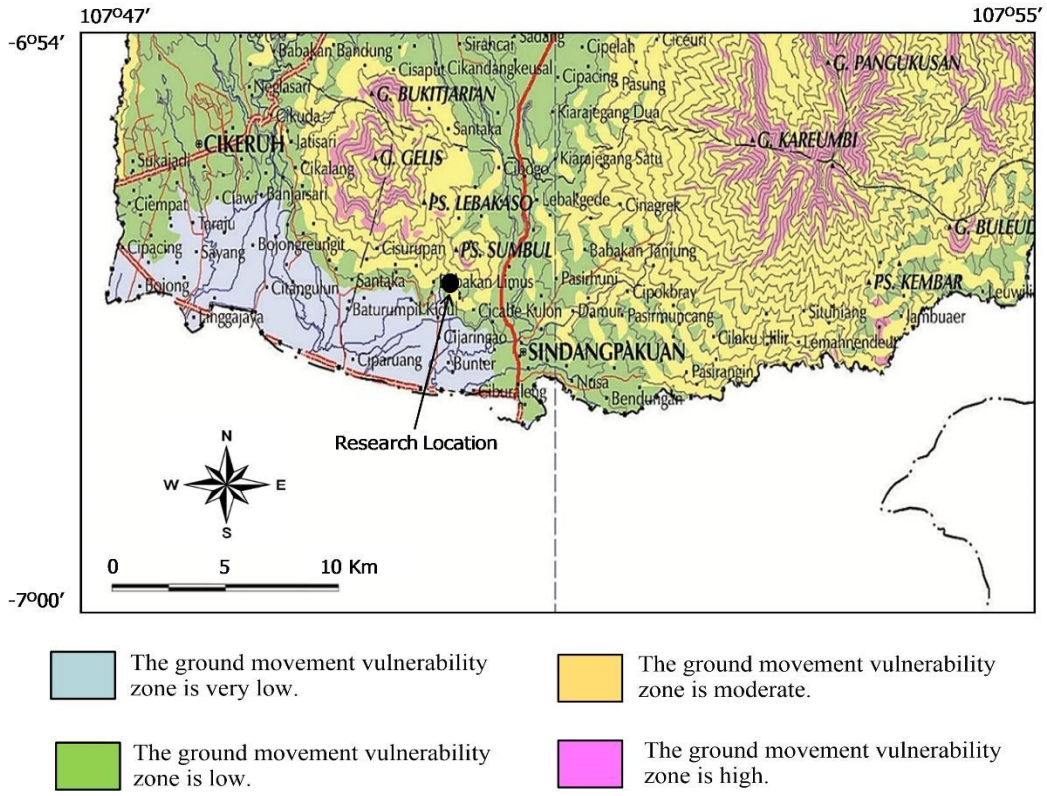

Figure 1 Vulnerability to landslide zone map of the study area, modified from vulnerability to landslide zone map of Sumedang Regency, West Java Province [22].

According to the stratigraphy [23], the research area is located within the Unconsolidated Young Volcanic Products Formation (Qyu), which consists of tuffaceous sand, lapilli, breccia, lava and agglomerate. This formation is partially derived from Mount Tangkubanparahu and Mount Tampomas. It is situated between Sumedang and Bandung, forming small plains and low hills covered by grayish-yellow and reddish soils. Regionally, the research area is dominated by volcanic rocks, including the presence of Lava from Volcanic Activity (Qvl) to the north, Unconsolidated Old Volcanic Products (Qvu) to the east, and Lake Deposits (Ql) to the south, consisting of tuffaceous sandstone, tuffaceous clay and tuffaceous gravel. Mapping conducted in the research area has identified outcrops of weathered basalt rocks to the west of the study site. These basalt rocks are believed to function as sliding planes due to their impermeable nature, which has resulted in the occurrence of fractures in the rocks or soil at the research location. The geological map of the research area is shown in **Figure 2**.

The occurrence of soil fractures in the research area is influenced by the development of fault structures in the vicinity. One active fault structure in the vicinity of the research area is the Cileunyi-Tanjungsari Fault, located to the north. The Cileunyi-Tanjungsari Fault has an orientation of northeast-southwest, extending from Tanjungsari to Cileunyi, and is believed to continue further to the Bandung Basin. The Cileunyi-Tanjungsari Fault is divided into 2 segments: The western segment with a length of

6.69 km and the eastern segment with a length of 11.28 km. This fault cuts through the units of old volcanic rocks, young volcanic rocks and the Bandung Lake deposits. Another active fault in the vicinity of the research area is the Cicalengka Fault, located to the south. The Cicalengka Fault has a northeast-southwest orientation, nearly parallel to the Cileunyi-Tanjungsari Fault, and extends from the southern part of Cicalengka to the eastern slope of Mount Malabar.

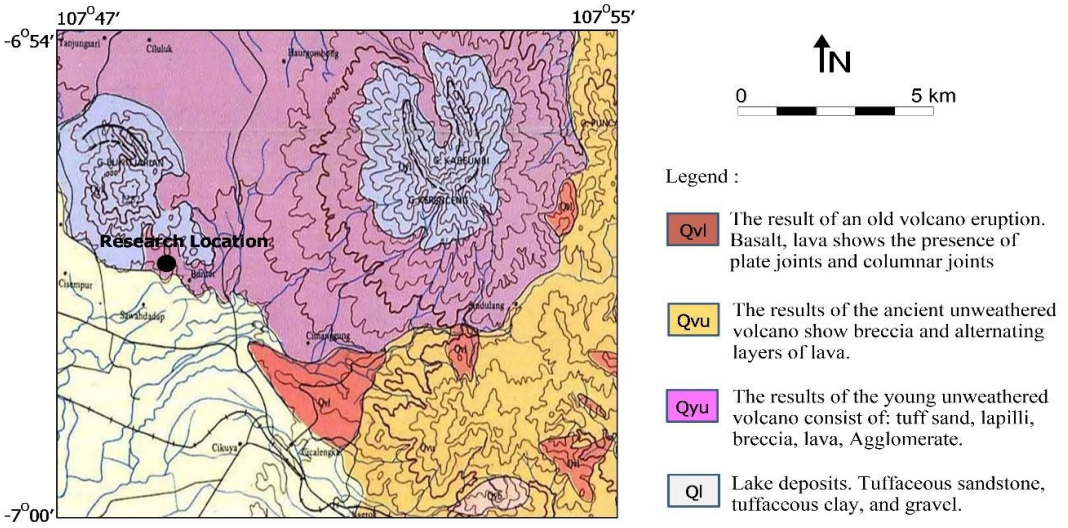

Figure 2 Geological map of the study area, modified from Bandung Sheet geological map [23].

Research methodology

In **Figure 3**, the flowchart illustrates the methodology used in the research. The required input data for this study is electrical resistivity tomography (ERT) data. Modeling is carried out using inversion methods based on ERT data that has been supplemented with topography (elevation) until ERT profiles and resistivity values at various depths are obtained.

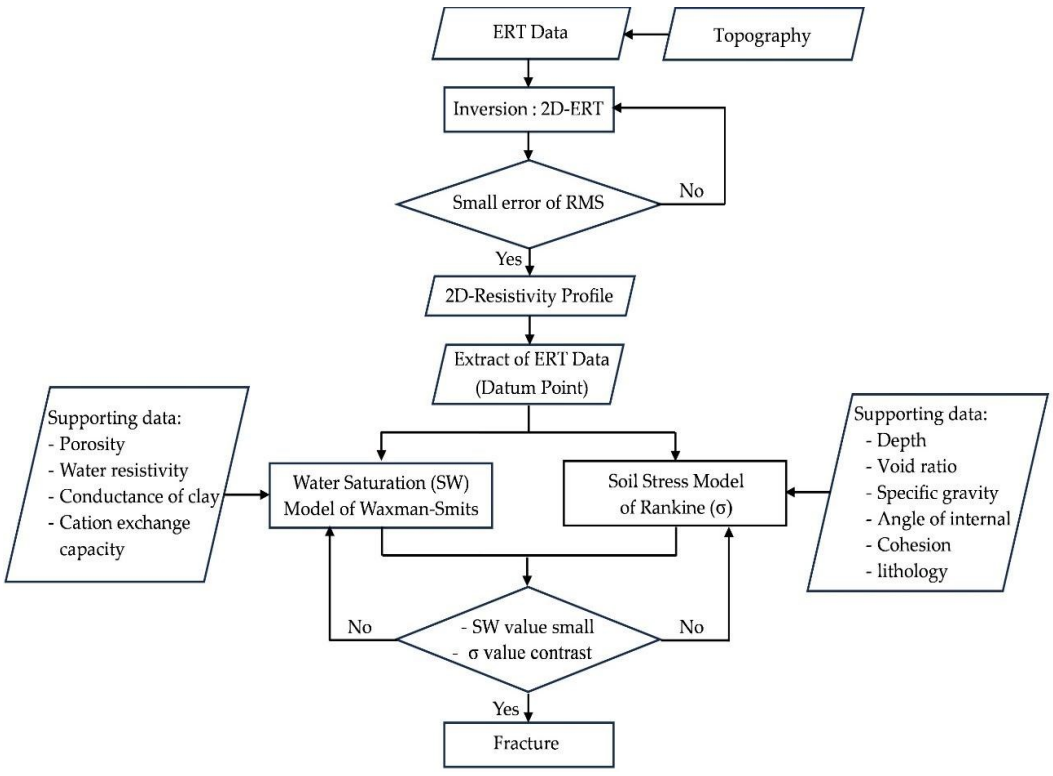

Figure 3 Flowchart of the proposed methodology.

Subsequently, to obtain information about ground fractures, the process involves calculating water saturation and soil pressure based on ERT data. The method used for water saturation calculation is the Waxman-Smits method, while the method used to calculate soil pressure is the Rankine method. Supporting data required for calculating water saturation includes: Porosity data, water resistivity, clay conductivity and cation exchange capacity. Supporting data required for soil pressure calculation includes: Void ratio data, specific gravity, depth, internal friction angle, cohesion and lithology.

Electrical Resistivity Tomography (ERT)

The geophysical method used in this research is Electrical Resistivity Tomography (ERT). ERT is a method for measuring the resistivity of the subsurface by using multiple electrodes on the ground surface. It provides lateral and vertical variations in resistivity distribution beneath the surface, allowing for the imaging of subsurface rock structures. ERT imaging can observe fracture patterns and soil propagation [24], including the formation of fractures involving soil mechanical parameters [25]. The ERT method is also effective in observing infiltration and determining the potential saturated and unsaturated zones in rocks [26]. It can visualize 3D unsaturated water flow in cement-based materials with separate fractures [27]. The selection of the ERT method in this research is based on the hypothesis that fractured zones and soil displacement planes have resistivity contrasts compared to the surrounding rock. The ERT method can also explain the relationship between resistivity of fractures and water saturation and soil stress, where the values of water saturation and soil stress are derived from ERT data [14-17].

The principle of ERT measurement involves injecting direct current into the ground through 2 current electrodes, while the resulting voltage response is measured using 2 potential electrodes [28]. The data obtained in Electrical Resistivity Tomography (ERT) measurements are the apparent resistivity values. The electrode configuration used in ERT data acquisition is the Dipole-Dipole configuration, chosen for its high lateral and vertical data resolution. The Dipole-Dipole configuration and the geometry of the datum points are shown in **Figure 4**.

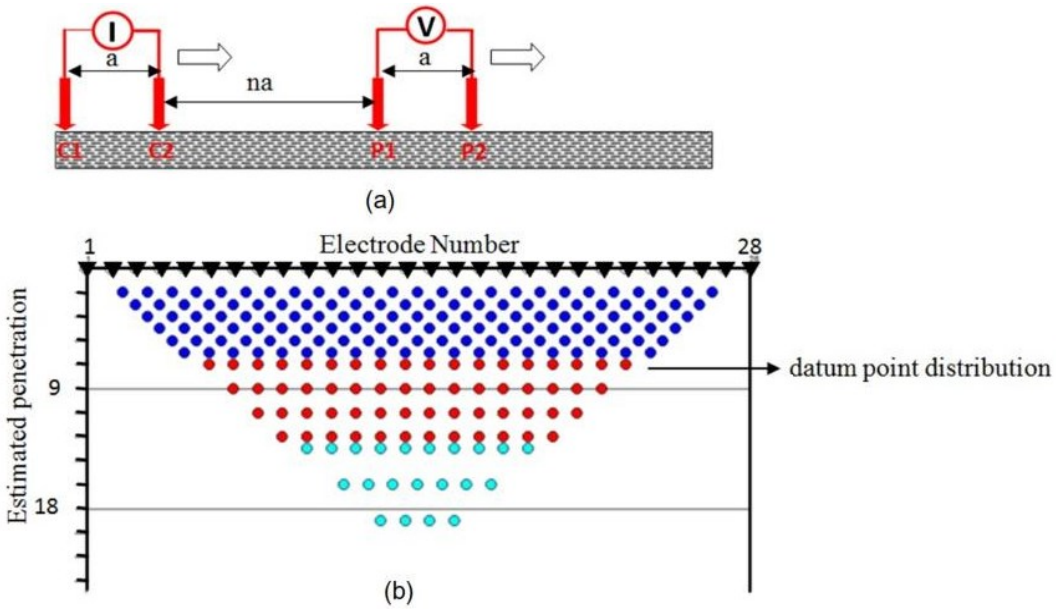

Figure 4 (a) Dipole-dipole electrode configuration. C1 and C2: Current electrodes, P1 and P2: Potential electrodes, a: Electrode spacing and na: Measurement interval. (b) Distribution of datum points and estimated penetration depths.

In **Figure 4,** C1 and C2 represent the 2 electrodes for current injection, while P1 and P2 are the electrodes for voltage measurement. Each electrode is spaced at a distance of a, and the measurements are repeated at intervals of na (n = 1, 2, 3 and so on). As the value of n increases, the current penetration becomes deeper, resulting in a resistivity pseudosection. The geometry factor (K) of the Dipole-Dipole configuration can be calculated using the equation below:

$$K = n(n+1)(n+2)\pi a \quad (1)$$

The geometric factor refers to the configuration or arrangement of current and potential electrodes used in Electrical Resistivity Tomography (ERT) measurements. The resistivity value can be calculated using the equation below:

$$\rho_s = n(n+1)(n+2)\pi a \frac{\Delta V}{I} \quad (2)$$

The apparent resistivity (ρ_s)is the calculated result derived from the voltage and current obtained in Electrical Resistivity Tomography (ERT) measurement points determined by the specific configuration of the electrode positions in the field.

The resistivity modeling was performed using the inversion software Res2DInv to generate the ERT profile model. The level of model error is indicated by the root mean square (rms) error, which represents the correlation between the observed pseudosection of apparent resistivity and the calculated pseudosection of apparent resistivity.

The equipment used for ERT measurements was the Supersting R8 with 28 electrodes. The ERT survey comprises 6 lines as follows: Line AB, oriented Northeast-Southwest, with a length of 120 m and an electrode spacing of 8 m. Line CD, oriented Northeast-Southwest, with a length of 136 m and an electrode spacing of 8 m. Line EF, oriented Northeast-Southwest, with a length of 94.5 m and an electrode spacing of 8 m. Line GH, oriented North-South, with a length of 120 m and an electrode spacing of 3 m. Line IJ, oriented North-South, with a length of 120 m and an electrode spacing of 3.5 m. Finally, line KL, oriented Northwest-Southeast, with a length of 120 m and an electrode spacing of 3.5 m. The positions of each Electrical Resistivity Tomography (ERT) measurement line are indicated in **Figure 5**.

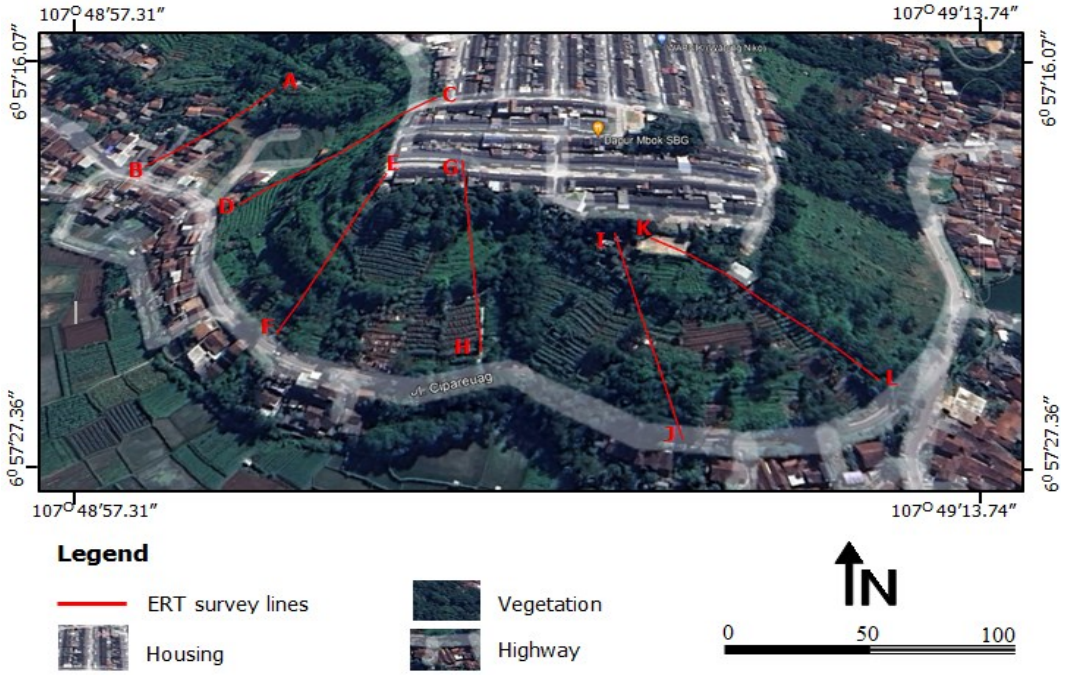

Figure 5 Map of the ERT measurement line in the research area, West Java, modified from Google Earth. The difference in elevation between the foot of the slope and the crown of the slope is 20 - 35 m, depending on the position of each ERT line.

Water saturation method

The resistivity data obtained from the inversion modeling is used as input data for petrophysical modeling of water saturation. The software used for water saturation modeling is Surfer v26. The relationship between resistivity and water saturation can be explained using the Waxman-Smith model. This model has advantages compared to the Archie model. It exhibits excellent accuracy in determining water saturation in clay-containing formations [29,30]. Moreover, the Waxman-Smits model can explain the influence of clay in contributing to cation exchange, thereby enhancing the formation's conductivity [16]. Conversely, the Archie model is only applicable for determining water saturation in formations without clay.

The equation for the Waxman-Smith model is as follows:

$$S_w = \left[\frac{R_w}{\emptyset^m R_t\left(1+R_w B\frac{Q_v}{S_w}\right)}\right]^{\frac{1}{n}} \quad (3)$$

In Eq. (3) R_w is the resistivity of water, R_t is the total resistivity, m is constant characterizing cementation, $\emptyset$ is the porosity of the rock, B is the clay conductivity, Q_v is the cation exchange capacity, S_w is the water saturation, and n is the saturation exponent.

Active soil stress (the Rankine method)

The soil stress present at the research site is classified as active lateral soil stress. Active lateral soil stress occurs due to the soil thrust from the top of the slope/embankment, resulting in soil displacement and reaching an active condition where the soil elements will move away from the soil mass. If the soil movement is significant, a potential sliding plane will form within the soil mass, causing the soil to move forward and downward. One of the methods used to calculate active lateral earth stress is the Rankine method. Rankine developed a theory of lateral soil stress based on the concept of plastic equilibrium. Plastic equilibrium refers to a state that causes every point within the soil mass to move towards a state of soil failure [31].

In the Rankine method, a soil mass is confined by walls with a smooth surface that extends to an infinite depth (**Figure 6**). The soil elements located at a depth z will experience vertical stress (σv) and horizontal stress (σh), while the shear stress on vertical and horizontal planes is neglected.

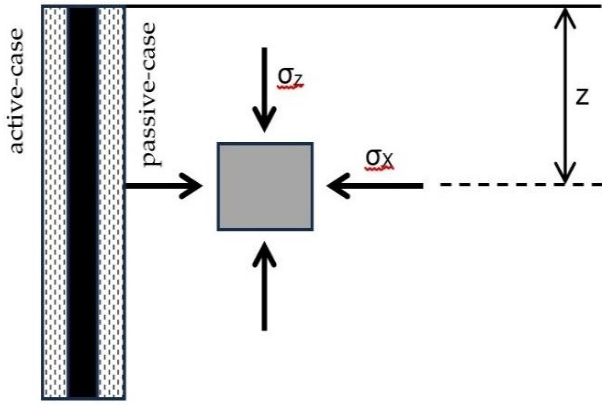

Figure 6 Stress conditions on soil elements behind the wall.

The equation to calculate vertical stress (σv) is as follows:

$$\sigma'_v = \gamma z. \quad (4)$$

In this expression, γ is bulk density of soil, and z is the depth of the soil layer from the ground surface to point z. The equation to calculate the active soil stress coefficient is as follows:

$$K_a = tan^2\left(45 - \frac{\emptyset\prime}{2}\right) \quad (5)$$

where ($\emptyset$) is the internal friction angle, the equation to calculate active soil stress σ'_a is as follows:

$$\sigma'_a = \sigma'_v K_a - 2c'\sqrt{K_a} \quad (6)$$

here, c represents the cohesion of the soil. The software used to visualize the lateral earth stress models was Surfer v26.

Results and discussion

ERT measurements were conducted from December 15, 2022, to December 22, 2022, along 6 profiles. The length of each profile varied between 94.5 - 136 m, depending on the slope length. The list of ERT profiles is shown in **Table 2**.

Table 2 ERT measurement line in the research area, West Java.

Line	Length of line (m)	Orientation
AB	120	NorthEast-SouthWest
CD	136	NorthEast-SouthWest
EF	94.5	NorthEast-SouthWest
GH	120	North-South
IJ	120	North-South
KL	120	NorthWest-SouthEast

The fracture zones can be identified from the water saturation model and lateral earth stress model based on ERT data. Water saturation is calculated using the Waxman-Smits equation, while lateral earth pressure can be indirectly determined by estimating lithology through the approach of resistivity values obtained from ERT data.

Analisis of Electrical Resistivity Tomography (ERT) profile

The ERT data obtained from the measurements consist of 6 profiles with a range of resistivity values between 5 and 3,500 Ω·m. The range of resistivity values obtained from ERT measurements indicates the type of rock (lithology), the presence of saturated water layers and indications of fractures. The high or low resistivity values of the soil are controlled by the water content and the presence of clay.

The resistivity profiles from the inversion modeling are shown in **Figure 7** (indicating fractures) and **Figure 8** (no indications of fractures). In the resistivity profile A-B (**Figure 7(a)**), a fracture zone is observed at a distance of 88 m (indicated by an arrow) with a resistivity value of 465 Ω·m. The high resistivity value in the fracture zone is attributed to poor electrode contact (both current and potential) with the soil or partial contact. This fracture zone was formed due to soil movement caused by the infiltration of rainwater into the ground. Rainwater flows as groundwater towards the lower part of the slope. When the rainfall stops and the water supply ceases, the soil becomes dry and starts to fracture, forming fracture zones. In the lowermost layer, at a depth of > 10 m, there is a very high resistivity value (> 1,460 Ω·m), which indicates bedrock instead of fractures. This high resistivity value is consistent with the local geological data, which indicates the presence of lava (igneous rock) in the area, which is resistant and impermeable, resulting in high resistivity.

In the resistivity profile I-J (**Figure 7(b)**), indications of fractures are observed at the upper and middle parts of the section with resistivity values ranging from 300 - 640 Ω·m. In the resistivity profile E-F (**Figure 7(c)**), fracture zones are present at the top and bottom parts of the section with resistivity values ranging from 300 - 1,460 Ω·m. Additionally, indications of fractures are observed in the resistivity profile K-L (**Figure 7(d)**) at the top part with a resistivity value of 649 Ω·m. The variations in resistivity values observed in profiles: I-J (**Figure 7(b)**), E-F (**Figure 7(c)**) and K-L (**Figure 7(d)**) are related to the groundwater content, the presence of clay layers and the existence of gaps or voids in the soil. Soil layers with groundwater and clay content exhibit low resistivity values (< 91 Ω·m), whereas layers with gaps or voids (indicated by arrows) display high resistivity values (> 300 Ω·m) due to poor electrical contact between the current electrodes. In all 3 profiles, high resistivity values are also found in the bottommost layer, which is massive and characterized by the presence of hard rocks (bedrock).

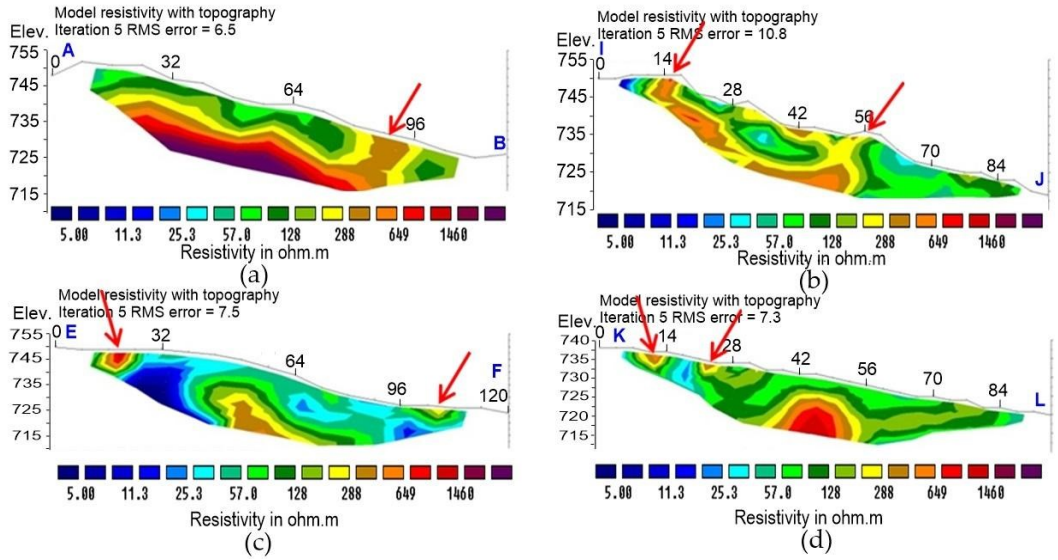

Figure 7 Resistivity profiles of line: A-B, E-F, I-J and K-L showing the presence of fracture zones in each profile.

The difference in the resistivity range of the fracture zones is related to the contact between the current electrodes and the soil. The less contact there is between the electrodes and the soil, the higher the resistivity value will be. In the lowermost layer of all 3 profiles, high resistivity values (> 649 Ω·m) are obtained, indicating the presence of bedrock. This bedrock is composed of impermeable and highly compacted lava from igneous rock, resulting in high resistivity. The bedrock in the I-J resistivity profile (**Figure 7(b)**) and E-F resistivity profile (**Figure 7(c)**) has a specific slope pattern, where the upper part of the bedrock can act as a potential sliding plane. The presence of this sliding plane can accelerate soil movement and the occurrence of soil fractures.

In **Figure 8**, resistivity profiles of line C-D and G-H are shown, where no fractures or unstable soil conditions were found in both tracks. In **Figure 8(a)**, there is a bedrock (highlighted in red, resistivity value > 649 Ω·m) in the middle of the profile, which serves to support the soil load from the upper part of the slope. Therefore, the soil condition in this track is relatively stable, and no fractures were observed. In **Figure 8(b)**, there are some lensing patterns near the surface with small resistivity values around 128 Ω·m, which are suspected to be small boulders. However, no fractures were found in the lower part of the profile.

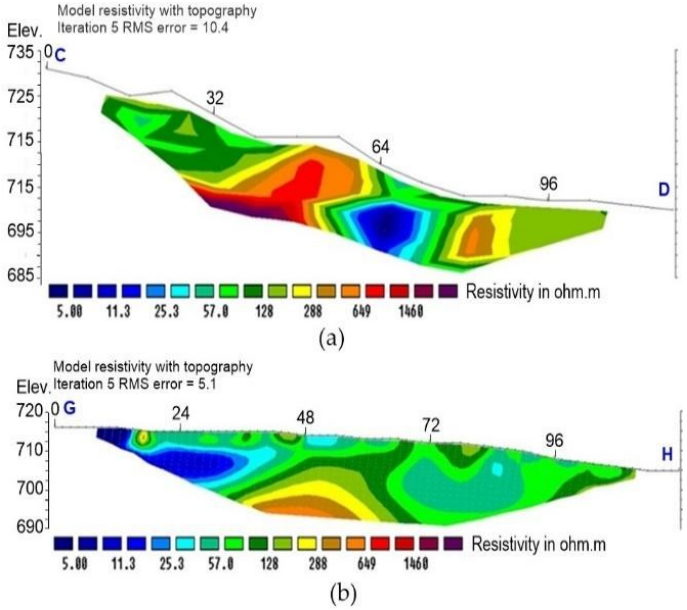

Figure 8 Resistivity profiles of line: C-D and G-H, indicating stable soil layers without any fractures.

Based on the correlation between resistivity values and local geology, the resistivity values and lithology of the fracture zones are obtained as shown in **Table 3**.

Table 3 Resistivity value of fracture and lithology [4,28,32].

Lithology/Fracture	Resistivity (Ω·m)
Bedrock	400 - 1,460
Fracture	> 251
Silty sands	91 - 250
Clayey silt	≥ 90

The resistivity values of the rocks in **Table 1** were used when indirectly correlating resistivity with effective soil stress, which will be discussed further in subsection relationship between resistivity and soil stress.

The petrophysical relationship between water saturation and resistivity

The petrophysical model used to explain the indication of fractures is the Waxman-Smith model (1968). To calculate water saturation (SW) using the Waxman-Smits model in Eq. (6), several measurement data are used, including water resistivity (Rw = 10 Ω·m), inversion resistivity, porosity (Ø = 0.5). Other data obtained from the literature include B = 3.5 S, Qv = 0.09 meq/mL, m = 1.8 and n = 2.1 [29]. These data are then substituted into Eq. (6), resulting in the SW equation for water saturation using the Waxman model as follows:

$$S_w = \left[\frac{8.4}{R_t}\right]^{0.48} \quad (7)$$

Based on Eq. (7), the graph showing the relationship between resistivity and water saturation is presented in **Figure 9**.

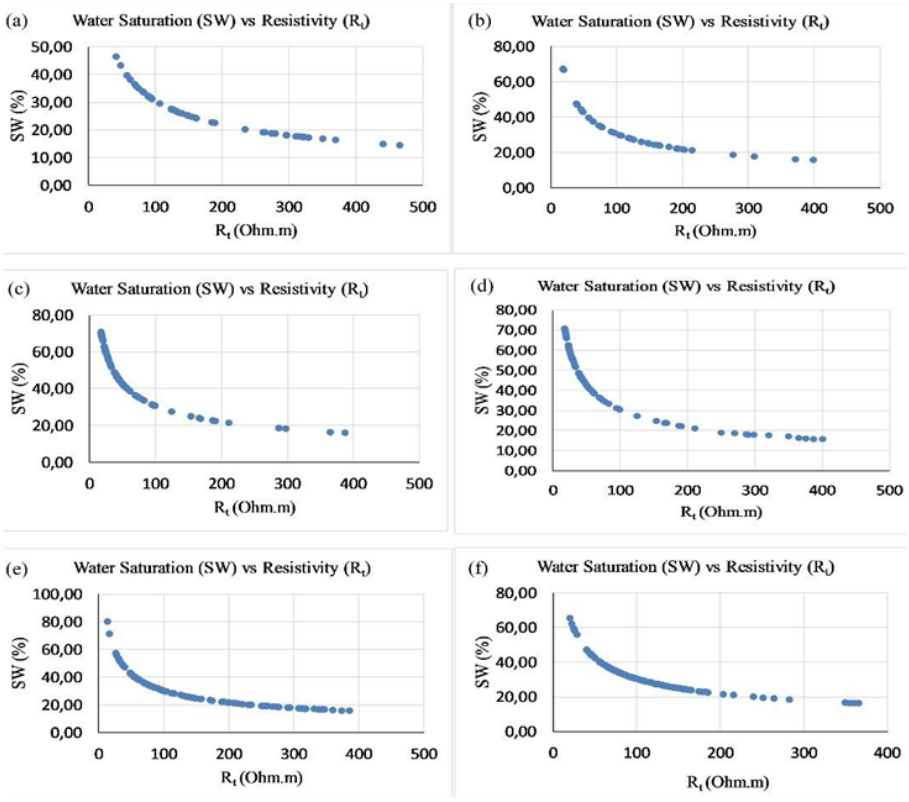

Figure 9 Graph of water saturation (SW) vs resistivity (R_t) on the line: A-B (**Figure 7(a)**), I-J (**Figure 7(b)**), E-F (**Figure 7(c)**), K-L (**Figure 7(d)**), C-D (**Figure 7(e)**) and G-H (**Figure 7(f)**).

From the graph, it can be observed that the relationship between water saturation and resistivity is non-linear. The resistivity values of the soil decrease as the water saturation increases.

Overall, based on the 6 graphs in **Figure 9**, low resistivity values (< 75 Ω·m) indicate relatively wet soil layers with water saturation values ranging from 35 - 80 %. For soil with low water content (somewhat dry soil) and water saturation values below 20 %, the resistivity values are higher, ranging from 280 - 480 Ω·m. The high resistivity values in this case are attributed to the low water content in the soil, indicating the presence of soil fractures. As the soil condition becomes drier within the fractures, the resistivity values increase, while the water saturation values decrease or approach 0.

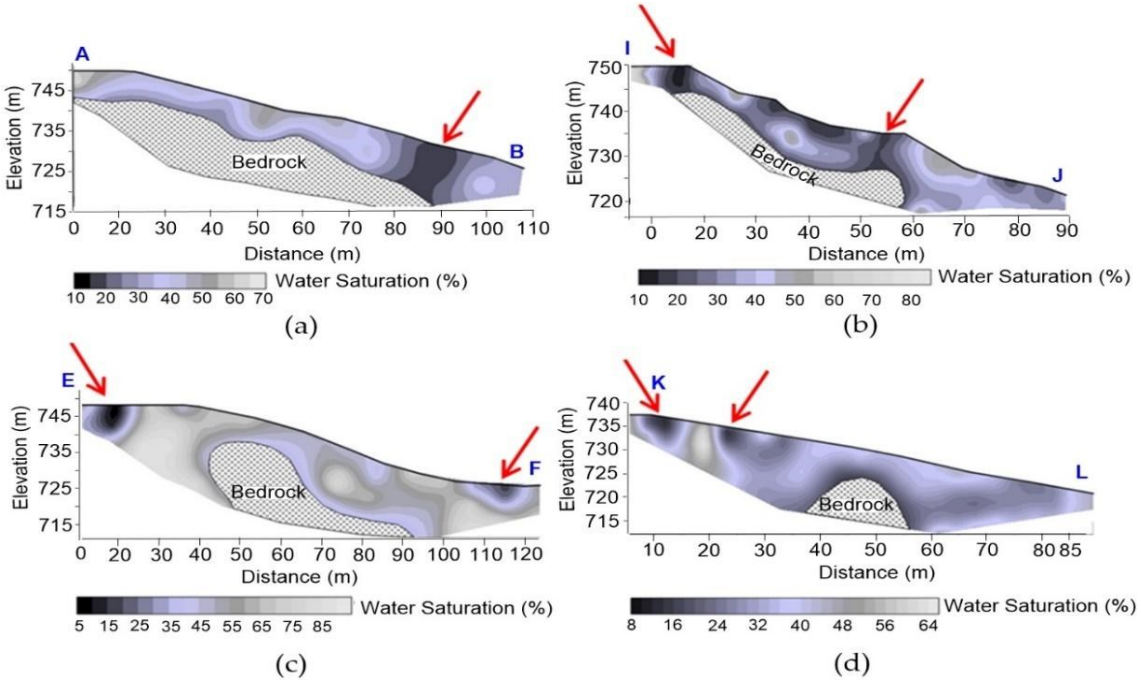

Figure 10 Waxman-Smits water saturation profile experiencing deformation (fractures).

Based on Eq. (7), the water saturation (Waxman-Smits) profiles are obtained (**Figures 10** and **11**). **Figure 10** shows the water saturation profile indicating the presence of a fracture zone. The fracture zone is identified in the water saturation profile with SW values < 15 % (indicated by red arrows). The smaller the SW value, the higher the level of fracturing. In the bottom layer, there is bedrock composed of lava (igneous rock). The bedrock is impermeable, so its upper part can act as a sliding plane. The presence of a sliding plane can accelerate soil fracturing [8,13] due to various factors: 1) The increased stress concentration: Sliding planes can concentrate stress within specific areas, intensifying the stress on the soil and leading to fracturing under excessive loads. 2) The reduced shear strength: Sliding planes often indicate weakened or compromised layers within the soil. These planes can act as zones of weakness, reducing the shear strength of the soil and making it more susceptible to fracturing. 3) The propagation of fractures: Sliding planes can serve as pathways for fractures to propagate through the soil mass. Once initiated along these planes, fractures can spread more rapidly, causing soil to break apart more easily. 4) The water movement: Sliding planes can facilitate water movement within the soil. Water ingress or accumulation along these planes can weaken soil cohesion, leading to increased fracturing as the soil becomes more saturated and loses its stability. 5) The shear stress redistribution: The presence of a sliding plane can redistribute shear stresses within the soil. This redistribution can alter stress patterns, inducing fractures and causing soil to break apart more readily. Overall, sliding planes act as critical zones that alter the mechanical behavior and stability of the soil, often leading to accelerated fracturing and instability.

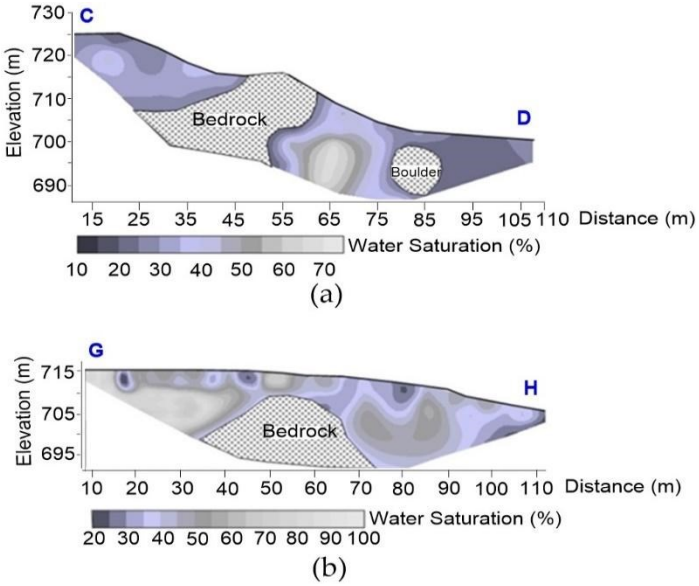

Figure 11 Unfractured Waxman-Smits water saturation profile.

In **Figure 11**, it shows the water saturation profile that does not indicate the presence of any fractures. In profiles C-D and G-H, there is no contrast in SW values indicating the existence of a fracture. The SW values in both profiles are relatively high, ranging from 30 to 60 % in profile C-D and from 30 to 70 % in profile G-H. SW values vary, indicating the degree of soil fracturing; the higher the SW value, the lower the degree of soil fracturing.

Relationship between resistivity and soil stress

The effective stress of the soil can be indirectly determined through the relationship between void ratio and resistivity values obtained from ERT modeling. The void ratio values are obtained from literature and adjusted according to the type of soil, which is estimated based on the resistivity values from the ERT profiles. These resistivity values are also used to estimate the saturated and unsaturated soil layers. The condition of saturated/unsaturated is necessary in determining the effective stress of the soil, as the calculation formula for effective stress differs based on this condition. The effective stress of the soil is calculated at each datum point along the ERT profiles, except for specific points located within the bedrock layer. To calculate the effective soil stress, several assumptions and data from literature and measurements (**Table 4**) are used.

Table 4 Values of soil parameters for effective soil stress.

Lithology	soil angle of internal friction (degree)	Soil cohesion (kg/cm^2)	Specific gravity (N/m^3)	Void ratio (%)
Clayey silt	23	0.35	2.62	1.22
Silty sands	30[a]	0.15[a]	2.68[a]	0.45[a]
Fracture zone	40[b]	0[b]	2.62	1.22

[a] [33,34]
[b] [35]

The profiles of effective soil stress calculated using Eq. (6) are shown in **Figures 12** and **13**. **Figure 12** represents the profile of effective soil stress, indicating the presence of soil fractures. Therefore, effective soil stress is an important parameter for controlling soil strength [36]. In this position, there is a contrast in lateral soil stress values, with low soil stress values < 5 KN/m^2 and high soil stress values ranging from 20 - 170 KN/m^2. The contrast in soil stress values will affect the soil strength. Soil with low soil stress values will move towards the slope due to the push from the soil with high soil stress values, resulting in soil displacement and the occurrence of fractures.

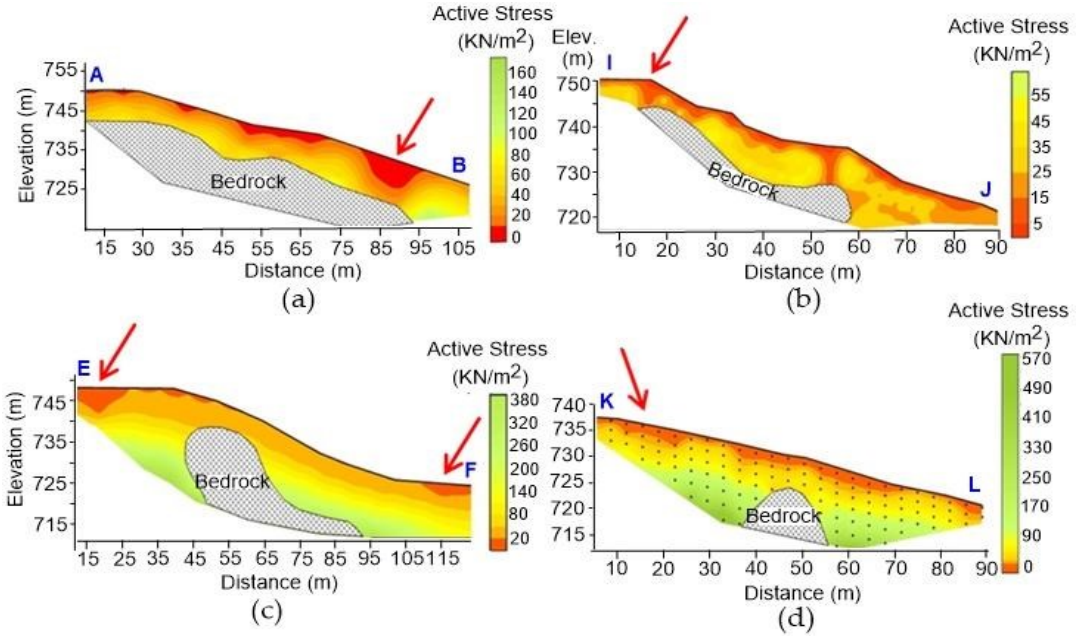

Figure 12 Profile of active soil stress indicating soil fractures caused by soil displacement.

In **Figure 12(a)**, at a distance of 90 m, there is an indication of a fairly wide fracture zone. The indication of the fracture at this position occurs due to the contrasting lateral soil stress values, resulting in a reduction in soil shear strength. At the foot of the slope at a distance of 105 m, the condition is relatively stable with nearly the same lateral soil stress value of 90 KN/m².

In **Figure 12(b)**, indications of fracture zones are present at the top of the slope (at a distance of 20 m) and the bottom of the slope (at a distance of 120 m). At the top and bottom of the slope, there are contrasting values of soil stress, leading to soil displacement and the occurrence of fractures. In the underlying soil layers, at depths of 5 - 15 m, the soil conditions are relatively stable as the lateral soil stress distribution has nearly the same value of ± 120 KN/m^2. Similarly, at depths of 15 - 20 m, the active soil stress also has similar values ranging from 260 - 380 KN/m^2, indicating a relatively stable soil condition.

In **Figure 12(c)**, the active soil stress profile indicates unstable soil conditions. The lateral soil stress profile along line 5 shows a relatively high number of fractures, mainly due to the presence of soft soil (silt/clay). The soil is not compacted, has low shear strength, low permeability coefficient, and low bearing capacity. At a distance of 55 m, there is a contrast in soil stress values from the surface to a depth of 9 m. This contrast in soil stress can lead to soil displacement and the occurrence of soil fractures. At the top of the slope, at a distance of 15 m, there is also a contrast in soil stress values up to a depth of 5 m, indicating the presence of a fracture zone.

In **Figure 12(d)**, the active soil stress profile shows slightly less stable soil conditions at the top of the slope. Along line 6, the soil consists of both compacted and soft soil. At the top of the slope (at a distance of 15 m) and the bottom of the slope (at a distance of 90 m), there are indications of fractures characterized by less compacted soil and low bearing capacity. In the soil layers with depths ranging from 4 - 20 m, the conditions are relatively stable as the lateral soil stress values at those depths are almost the same.

Figure 13 illustrates the active soil stress profile in stable soil conditions without indications of fractures. In **Figure 13(a)**, at depths of less than 5 m, no indications of fractures were found. The active soil stress has a relatively consistent value of ± 30 KN/m^2 (orange color). At depths between 5 to 8 m, the soil condition is still stable (no soil fractures) with an active soil stress value of approximately ± 110 KN/m^2 (yellow color). At depths ranging from 8 to 18 m, the soil stress value increases to around ± 300 KN/m^2 (green color). However, lateral variations between data points are nearly the same, indicating the absence of soil fractures. Since there is no contrasting soil stress value, the soil conditions along the C-D section are relatively stable, and there are no indications of fractures.

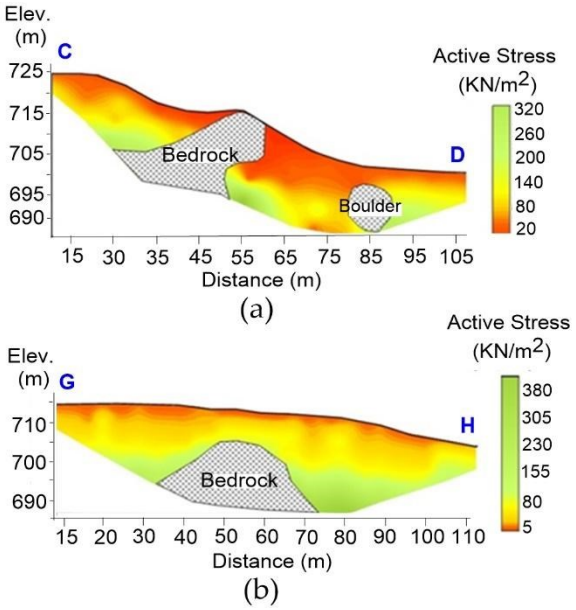

Figure 13 Shows the active soil stress profile under stable soil conditions without any fractures.

In profile G-H (**Figure 13(b)**), at depths of less than 3 m, no indications of soil fractures were found. This is evident from the relatively small soil stress value of about 5 KN/m^2 and the almost consistent lateral stress values at that depth. At depths between 3 to 12 m, the soil stress value increases to around 75 KN/m^2 (yellow color), while the lateral distribution of soil stress remains relatively consistent. Therefore, no indications of soil fractures were found at this depth either. Moving deeper, between depths of 12 to 22 m, the soil stress value continues to increase to approximately 330 KN/m^2, with similar lateral stress variations (yellow color). Consequently, the soil conditions remain stable at this depth, and there are no indications of fractures.

The social implications of ERT survey on the surrounding community

Survey of Electrical Resistivity Tomography (ERT) for slope fracture holds significant social implications, including: 1) Safe development planning: Information derived from resistivity measurements (ERT) concerning slope fractures allows for adapting development plans while considering risk factors. This can influence safer infrastructure construction, selection of building sites and creating safer spatial layouts for communities. 2) Community safety: Identifying slope fractures through resistivity measurements (ERT) helps mitigate risks of accidents and natural disasters like landslides or soil collapses. Enhanced understanding of slope structures allows for preventive measures and early warnings to protect local residents. 3) Increased public awareness: Information obtained from resistivity measurements can provide communities with a better understanding of the risks associated with slope fractures. This heightened awareness of dangers and knowledge about protective actions can empower individuals to safeguard themselves and their environment. 4) Improved Disaster Management: Accurate information from resistivity measurements can be utilized by authorities in emergency response planning and disaster management. This includes more efficient evacuations and post-disaster handling efforts.

Therefore, ERT surveys for slope fractures are not only crucial for scientific understanding but also have significant impacts on protecting and enhancing the quality of life for communities vulnerable to natural disasters.

Conclusions

The relationship between resistivity and water saturation to identify soil fractures can be comprehensively explained using the Waxman-Smits petrophysical model. The model was able to identify the fracturing mechanism based on the water saturation profile. Soil with a low water saturation value (5 - 15 %), indicating a very low water content, is susceptible to developing fractures. In this study, 1 type of soil identified to influence water saturation values is clayey silt with a resistivity value of less than 90 Ω·m. The clayey silt have a high cation exchange capacity (CEC). The clayey silt with a high CEC has a greater

ability to retain cations from the soil solution. The cations held by clay can reduce the amount of cations present in the soil solution, consequently impacting water saturation.

Based on the saturation versus resistivity graph, a non-linear relationship is obtained between water saturation and resistivity. In this relationship, the resistivity of the soil consistently decreases with increasing water saturation. This means that as the water saturation value decreases and the resistivity value increases, the likelihood of soil fractures also increases.

Soil fractures can also be identified by the contrasting soil stress values. The soil fractures have lower stress values (< 15 KN/m^2) compared to the surrounding soil. The difference in soil stress values affects the soil's strength. Soil with lower stress value has more tendency to easily shift or collapse due to the pushing force from the surrounding soil with higher stress values.

Acknowledgements

We would like to express our gratitude to Universitas Padjadjaran, Indonesia for funding this research through the Riset Disertasi Doktor Unpad (RDDU) 2020 scheme.

References

[1] R Baker. Tensile strength, tension cracks, and stability of slopes. *Soils Found.* 1981; **21**, 1-17.
[2] CS Tang, DY Wang, C Zhu, QY Zhou, SK Xu and B Shi. Characterizing drying-induced clayey soil desiccation cracking process using electrical resistivity method. *Appl. Clay Sci.* 2018; **152**, 101-12.
[3] D Smyl, MP Ghaz and A Seppanen. Detection and reconstruction of complex structural cracking patterns with electrical imaging. *NDT & E Int.* 2018; **99**, 123-33.
[4] A Hojat, D Arosio, VI Ivanov, L Longoni, M Papini, M Scaioni, G Tresoldi and L Zanzi. Geoelectrical characterization and monitoring of slopes on a rainfall-trigered landslide simulator. *J. Appl. Geophys*. 2019; **170**, 103844.
[5] X Zhou, P Bhat, H Quyang and J Yu. Localization of cracks in cementitious materials under uniaxial tension with electrical resistance tomography. *Construct. Build. Mater*. 2017; **138**, 45-55.
[6] S Alexsander, IB Mochtar and W Utama. Field validated prediction of latent slope failure based on cracked soil approach. *Lowland Tech. Int.* 2018; **20**, 245-58.
[7] G Jones, P Sentenac and M Zielinski. Desiccation cracking detection using 2-D and 3-D electrical resistivity tomography: Validation on a flood embankment. *J. Appl. Geophys.* 2014; **106**, 196-211.
[8] Y Fukomoto and T Shimbo. 3-D coupled peridynamics discrete element method for fracture and post-fracture behavior of soil-like materials. *Comput. Geotechnics* 2023; **158**, 105372.
[9] M Karsprzak, K Jancewicz, M Rozycka, W Kotwicka and P Migon. Geomorphology and geophysics-based recognition of stages deep-seated slope deformation (Sudetes, SW Poland). *Eng. Geol.* 2019; **260**, 105230.
[10] S Carpentier, M Konz, R Fischer, G Anagnostopoulos, K Meusburger and K Schoeck. Geophysical imaging of shallow subsurface topography and its implication for shallow landslide susceptibility in the Urseren Valley, Switzerland. *J. Appl. Geophys.* 2012; **83**, 46-56.
[11] J Gance, JP Malet, R Supper, P Sailhac, D Ottowitz and B Jochum. Permanent electrical resistivity measurements for monitoring water circulation in clayey landslide. *J. Appl. Geophys.* 2016; **106**, 196-211.
[12] S Uhlemann, PB Wilkinson, JE Chambers, H Maurer, AJ Merritt, DA Gunn and PI Meldrum. Interpolation of landslide movements to improve the accuracy of 4D geoelectrical monitoring. *J. Appl. Geophys.* 2015; **121**, 93-105.
[13] K Huang, Z Dai, Y Meng, F Yu, J Yao, W Zhang, Z Chi and S Chen. Mechanical behavior and fracture mechanism of red-bed mudstone under varied dry-wet cycling and prefabricated fracture planes with differentloading angles. *Theor. Appl. Fract. Mech.* 2023; **127**, 104094.
[14] Li, Z Hu, C Cai, X Liu, X Duan, J Chang, Y Lie, Y Mu, Q Zhang, S Zeng and J Guo. Evaluation method of water saturation in shale: A comprehensive review. *Mar. Petrol. Geol*. 2021; **128**, 105017.
[15] F Yongfei, R Horton, T Ren and JL Heitman. A general form of Archie's model for estimating bulk soil electrical conductivity. *J. Hydrol*. 2021; **597**, 126160.
[16] MW Lee. *Connectivity equation and shaly-sand correction for electrical resistivity.* United States Geological Survey, Virginia, United States, 2011.
[17] NJ George, AE Akpan and FS Akpan. Assessment of spatial distribution of porosity and aquifer geohydraulic parameters in parts of the Tertiary - Quaternary hydrogeoresource of south-eastern Nigeria. *NRIAG J. Astron. Geophys.* 2017; **6**, 422-33.

[18] SA Shah, SH Shah, A Bibi, QK Jadoon and K Latif. Petrophysical evaluation using the geometric factor theory and comparison with archie model. *J. Nat. Gas Sci. Eng.* 2020; **82**, 103465.
[19] M Oraby. Evaluation of the fluids saturation in a multi-layered heterogeneous carbonate reservoir using the non-archie water saturation model. *J. Petrol. Sci. Eng*. 2021; **201**, 108495.
[20] BMKG, Available at: https://dataonline.bmkg.go.id/, accessed December 2023.
[21] RAV Zuidam. *Aerial photo-interpretation in terrain analysis and geomorphology mapping*. Smith Publisher, The Hague, Netherlands, 1983.
[22] Pusat Vulkanologi dan Mitigasi Bencana Geologi. *Vulnerability to landslide zone map of Sumedang Regency, West Java Province.* Center for Volcanology and Geological Hazard Mitigation, Center for Volcanology and Geological Hazard Mitigation, West Java, Indonesia, 2020.
[23] PH Silitonga. *Geologic map of the Bandung Quadrangle Java, scale 1:100.000.* Geological Research and Development Centre, Bandung, Indonesia, 1994.
[24] N An, CS Tang, Q Cheng, DY Wang and B Shi. Application of electrical resistivity method in the characterization of 2D desiccation cracking process of clayey soil. *Eng. Geol*. 2020; **265**, 105416.
[25] S Bordoloi, J Ni and CWW Ng. Soil desiccation cracking and its characterization in vegetated soil: A perspective review. *Sci. Total Environ*. 2020, **729**, 138760.
[26] T Warsi, VS Kumar, R Dhakate, C Manikyamba, TV Rao and R Rangarajan. An integrated study of electrical resistivity tomography and infiltration method in deciphering the characteristics and potentiality of unsaturated zone in crystalline rock. *HydroResearch* 2019; **2**, 109 -18.
[27] D Smyl, R Rashetnia, A Seppanen and MP Ghaz. Can electrical resistance tomography be used for imaging unsaturated moisture flow in cement-based materials with discrete cracks? *Cement Concr. Res*. 2017; **91**, 61-72.
[28] WM Telford, LP Geldart and RE Sheriff. *Applied geophysics.* 2nd ed. Cambridge University Press, Newyork, 1990, p. 283-9.
[29] R Freedman and BE Ausburn. The Waxman-Smits equation for shaly sands: I. simple methods of solution; II. error analysis. *Log Anal.* 1985; **26**, 11-24.
[30] JA Al-Sudani, HK Mustafa, DF Al-Sudani and H Falih. Analytical water saturation model using capacitance-resistance simulation: Clean and shaly formations. *J. Nat. Gas Sci. Eng.* 2020; **82**, 103325.
[31] MD Braja. *Principles of geotechnical engineering*. 7th ed. Cengage Learning, Stamford, United States, 2010, p. 242-5.
[32] P Imani, G Tian, S Hadiloo and AA El-Raouf. Application of combined electrical resistivity tomography (ERT) and seismic refraction tomography (SRT) methods to investigate Xiaoshan District Landslide Site: Hangzhou, China. *J. Appl. Geophys*. 2021; **184**, 104236.
[33] MR Lindeburg. *Civil engineering reference manual for the PE exam*. Professional Publications, Belmont, United States, 2001.
[34] JW Koloski, SD Schwarz and DW Tubbs. Geotechnical properties of geologic materials. *Eng. Geol. Wash.* 1989; **1**, 19-24.
[35] D Adrian, IB Mochtar and NE Mochtar. Analisa sudut-geser-dalam tanah berbutir halus (cohesive soil) berdasarkan pendekatan cracked soil (*in Indonesian*). *Jurnal Teknik ITS* 2019; **8**, D74-D78.
[36] RD Holtz and WD Kovacs. *An introduction to geotechnical engineering*. Prentice-Hall, New Jersey, United States, 1981, p. 458-73.